

Supporting Information

Electrohydrodynamic Assembly of Ambient Ion-Derived Nanoparticles to Nanosheets at Liquid Surfaces

Depanjan Sarkar,^[a] Rajesh Singh,^[b] Anirban Som,^[a] C. K. Manju,^[a] Mohd Azhardin Ganayee,^[a]
Ronojoy Adhikari,*^[b,c] Thalappil Pradeep*^[a]

[a] Department DST Unit of Nanoscience (DST UNS) and Thematic Unit of Excellence (TUE),
Department of Chemistry, Indian Institute of Technology Madras Chennai – 60036, India.

[b] The Institute of Mathematical Sciences-HBNI CIT Campus, Chennai 600113, India.

[c] Department of Applied Mathematics and Theoretical Physics (DAMTP), Centre for Mathematical
Sciences University of Cambridge Wilberforce Road, Cambridge CB3 0WA, United Kingdom.

Table of Contents

| Item | Description | Page No. |
|------------------------------|------------------------------------------------------------------|----------|
| Materials and methods | Experimental details | S3 |
| Figure S1 | Schematic representation of the experimental set-up | S4 |
| Figure S2 | Wide range mass spectrum | S4 |
| Figure S3 | Detailed TEM EDS spectrum of Pd NP-NSs | S5 |
| Figure S4 | Plot of conductivity of the water, on which deposition happened, | S5 |

| | | |
|----------------------------|--------------------------------------------------------------------------------------------|-----|
| | vs deposition time | |
| Figure S5 | TEM images of Pd NP-NS before and after washing with DI water | S6 |
| Figure S6 | TEM image of Pd NP-NS synthesized by slow and fast electrospray deposition, respectively | S6 |
| Figure S7 | TEM images of Pd NPs formed after ESD of PdCl ₂ on formic acid solution | S7 |
| Figure S8 | TEM images of NP-NSs made of silver, gold and nickel | S7 |
| Figure S9 | TEM image of silver NP-NS made from silver perchlorate and silver nitrate | S7 |
| Figure S10 | TEM images of bimetallic NP-NSs | S8 |
| Figure S11 | Experimental and theoretical surface flows | S8 |
| Figure S12 | Mass spectrum of control experiments | S9 |
| Figure S13 | Mass spectrum collected from the reaction mixtures (serial no. 2-5) mentioned in Table S1 | S10 |
| Figure S14 | Mass spectrum collected from the reaction mixtures (serial no. 6-10) mentioned in Table S1 | S11 |
| Figure S15 | UV-Vis spectrum | S11 |
| Figure S16 | Stability and reusability of the catalyst | S12 |
| Table S1 | Structures of reactants and products | S10 |
| Theoretical details | Theoretical details of electrohydrodynamic flow | S13 |
| Video S1 | Video of fluid flow visualization | S15 |
| Video S2 | Video of fluid flow visualization at the surface | |

Experimental Details

Materials: All the chemicals used for the experiments were commercially available and were used without any purification. Palladium(II) chloride (PdCl_2), Silver acetate (AgOAc), gold(III) acetate (Au(OAc)_3) and tetrakis(triphenylphosphene) palladium(0) were purchased from Sigma Aldrich, India. 4-Methylphenylboronic acid, benzboronic acid, 4-bromophenol, 4-bromobenzoic acid, 4-bromoaniline, 4-iodophenol and 4-iodobenzoic acid were purchased from Avra Synthesis Pvt. Ltd. Hyderabad, India. HPLC grade acetonitrile (Sigma Aldrich, India) was used as solvent for all spray synthesis. A mixture of ethanol and locally available deionized water was used as the solvent for all the coupling reactions. Ethanol was purchased from Jiangsu Huaxi International Trade Co., Ltd., China.

Instruments: For all experiments, nanospray emitters were made using a micropipette puller (P-97) purchased from Sutter instrument, USA. Mass spectra were collected using an ion trap LTQ XL (Thermo Scientific, San Jose, California) mass spectrometer. For all mass spectrometry experiments, the spectrum was acquired both in positive and negative ion modes depending upon the functional groups of the compounds, in the mass range of m/z 50 to 500 under the following conditions: source voltage 3-5 kV, positive and negative (depending upon the analyte), capillary temperature 150°C , capillary voltage ± 45 V and tube lens voltage ± 100 V, \pm V are needed for positive and negative modes, respectively. Transmission electron microscopy (TEM) and high-resolution transmission electron microscopy (HRTEM) were performed using an accelerating voltage of 200 kV on a JEOL 3010, 300 kV instrument equipped with a UHR polepiece. A Gatan 794 multiscan CCD camera was used for image acquisition. EDS spectra were collected on Oxford Semi STEM system housed on the TEM. Samples were taken onto 300-mesh, carbon coated copper grids (spi Supplies, 3530C- MB) by scooping it from the liquid surface and drying under ambient conditions before examining in TEM. X-ray photoelectron spectroscopic (XPS) measurements were conducted using an Omicron ESCA probe

spectrometer with polychromatic MgK α X-rays ($h\nu=1253.6$ eV). Ultraviolet-visible (UV-Vis) spectra were measured with a PerkinElmer Lambda 25 instrument in the wavelength range of 200–1100 nm.

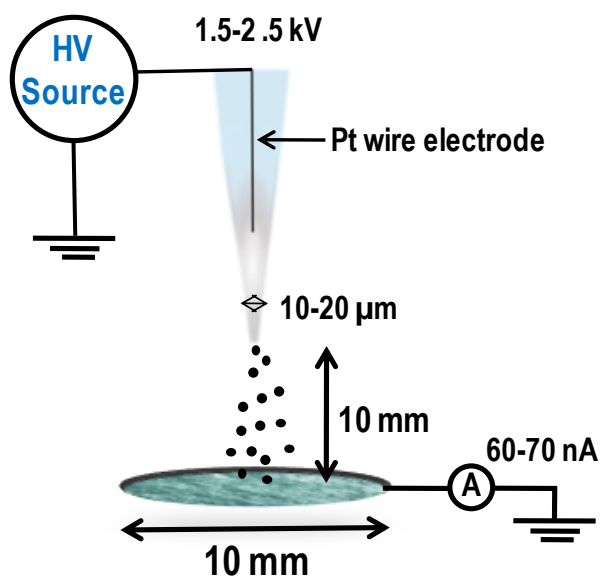


Figure S1. Schematic representation of the experimental set-up with dimensional details.

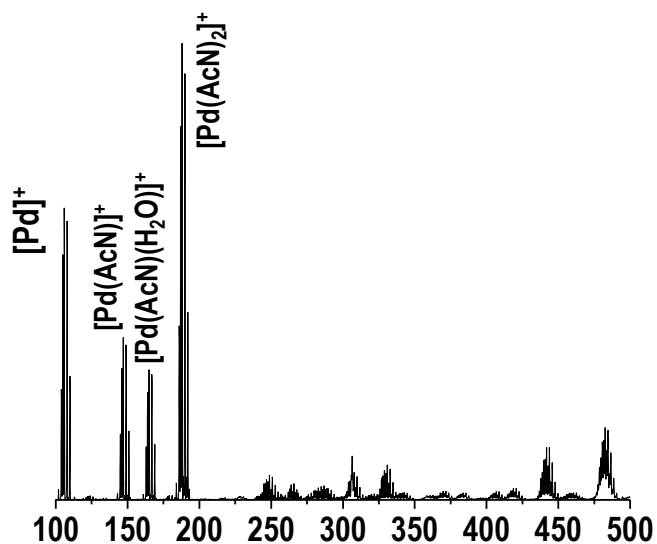


Figure S2. Mass spectrum collected from nESI of PdCl₂ showing the presence of salt clusters.

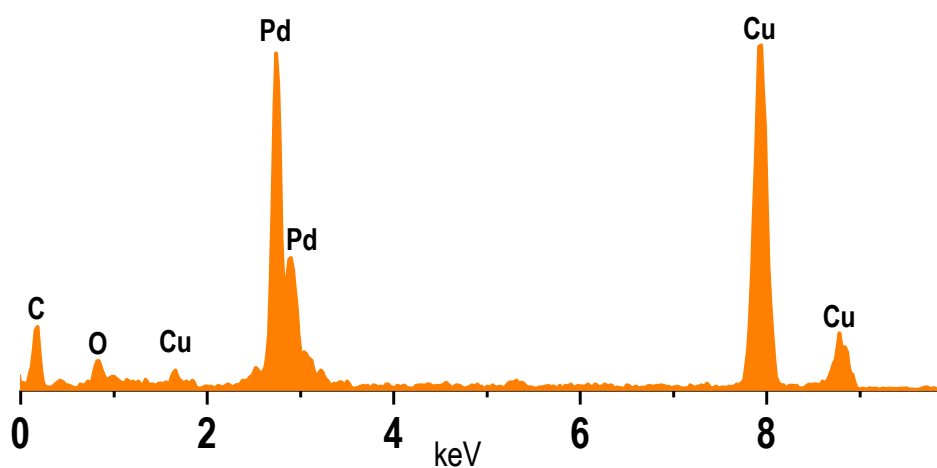


Figure S3. Detailed TEM EDS spectrum of Pd NP-NSs. Peaks due to C and Cu are from the TEM grid.

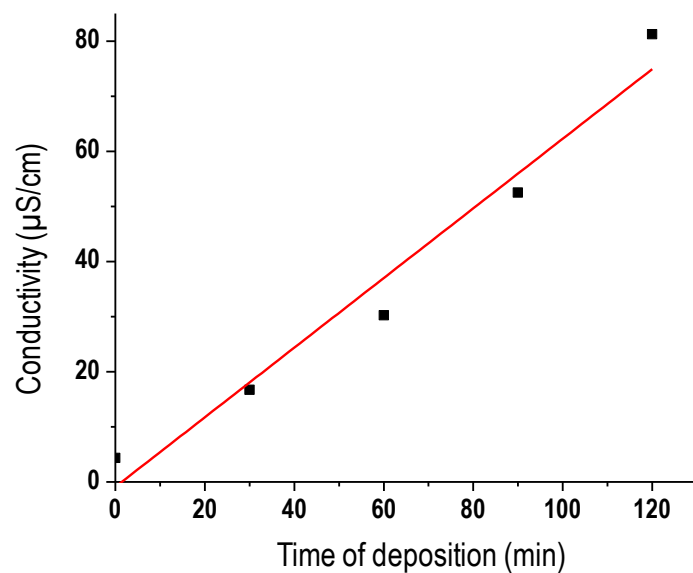


Figure S4. Plot of conductivity of the water, on which deposition happened, vs deposition time, showing linear enhancement in conductivity.

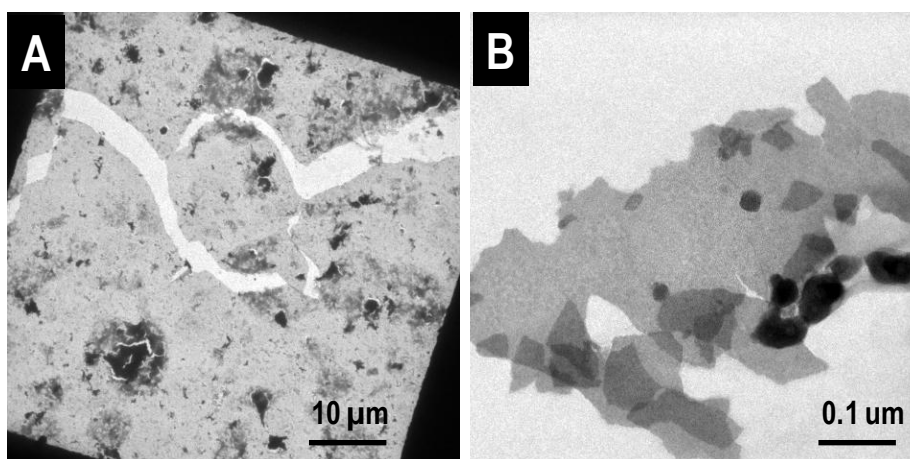


Figure S5. A) TEM image of as-synthesized Pd NP-NS over $80 \mu\text{m}^2$ area, B) Pd NP-NS after washing with DI water.

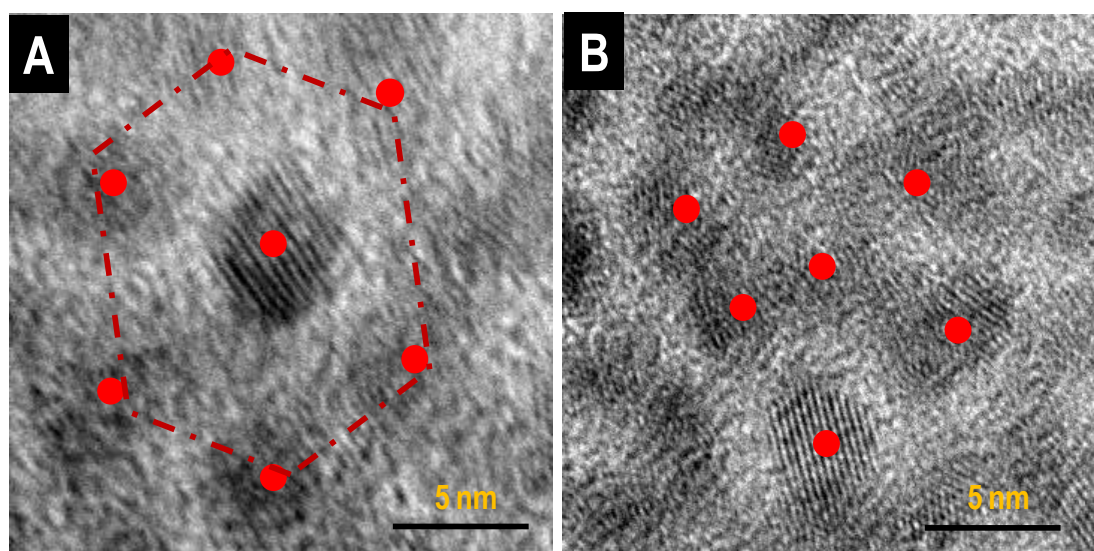


Figure S6. A and B show TEM image of Pd NP-NS synthesized by slow (30 nA) and fast (80 nA) electro spray deposition, respectively. Some particles are marked to show the regularity.

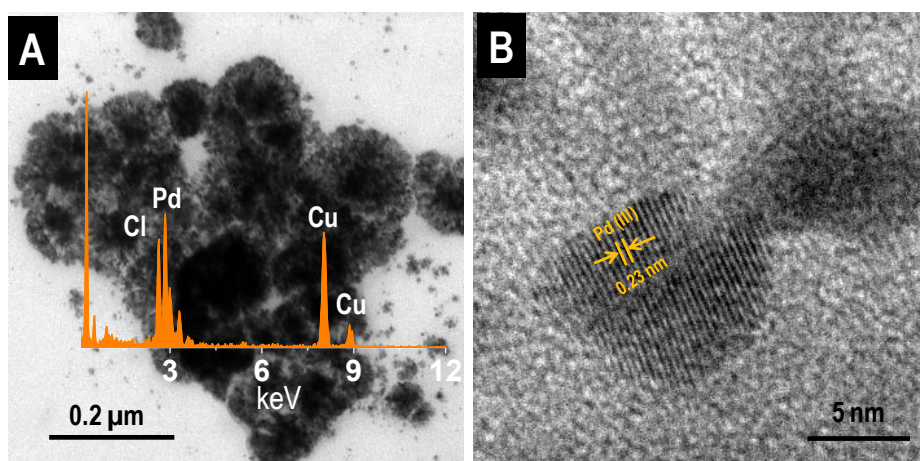


Figure S7. A) TEM images of Pd NPs formed after electrospray deposition of PdCl₂ on formic acid solution. In this case, sheet formation was not observed. EDS spectrum shows salt deposition. B) Part of the NPs are composed of metallic Pd as shown by the lattice planes (Pd).

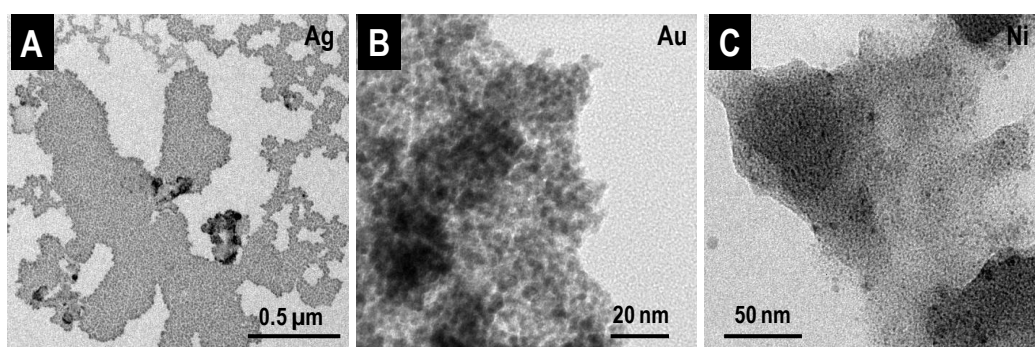


Figure S8. A, B and C) TEM images of NP-NSs made of silver, gold and nickel, respectively.

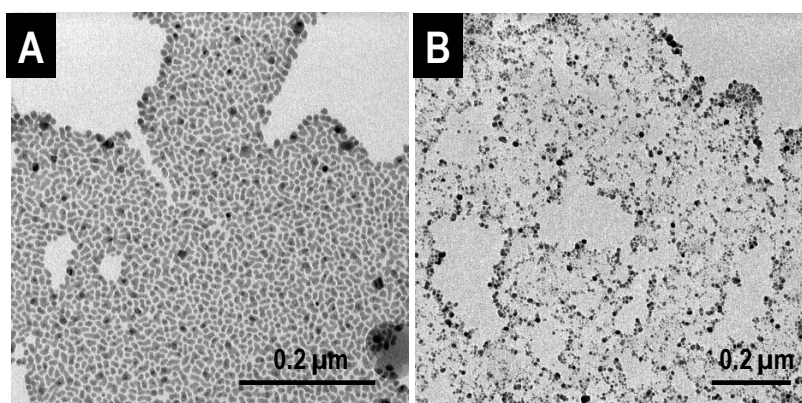


Figure S9. TEM image of silver NP-NS made from A) silver perchlorate and B) silver nitrate.

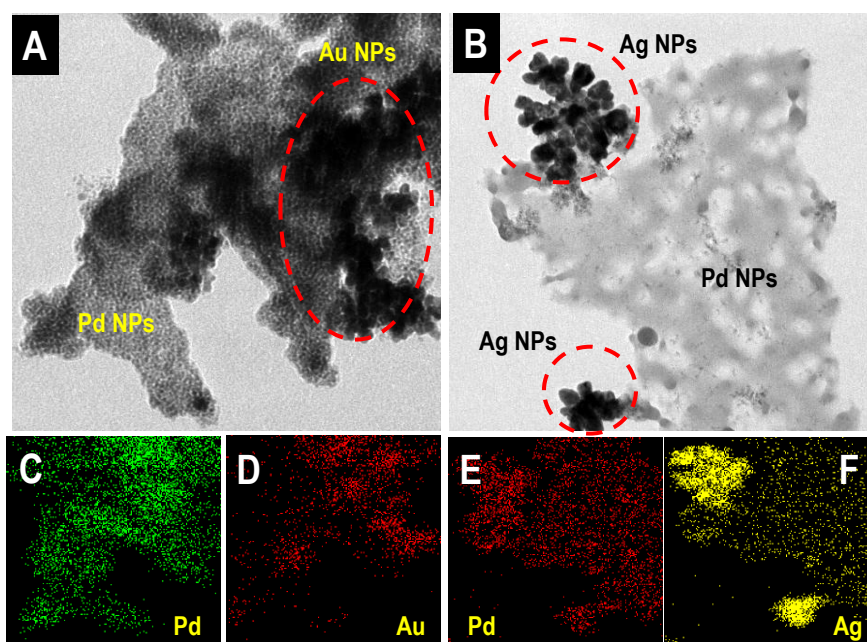


Figure S10. A) TEM image of Au-Pd NP-NS, B) TEM image of Ag-Pd NP-NS showing phase separated metal NPs. C-F) TEM EDS mapping of elements showing that the metal NPs aggregated themselves separately rather than making an alloy.

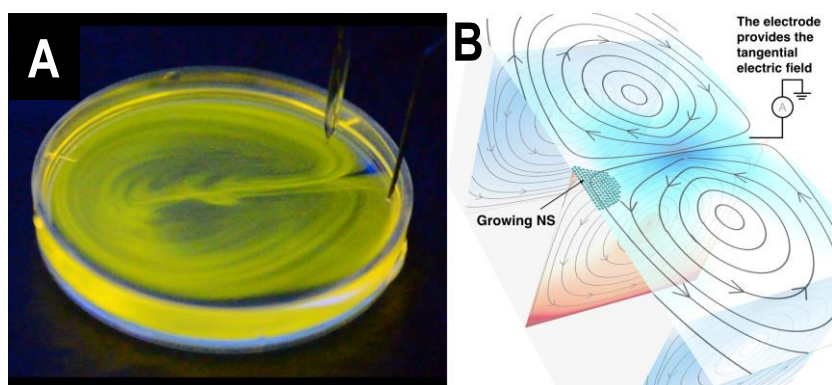


Figure S11. A) Dye visualization of the surface flow, B) theoretical streamlines showing the liquid flow at the surface. This surface flow drives nanoparticles away from the cathode and towards the opposite wall, while bulk flow recirculates the particles to the surface. The result is the growth of NS at the surface of the container.

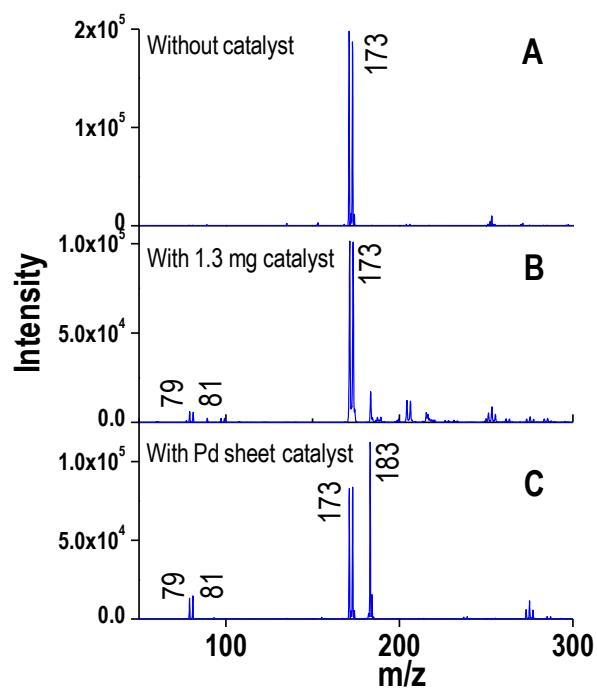


Figure S12. A) Mass spectrum collected from the reaction mixture of p-tolylboronic acid and p-bromophenol without catalyst, B) with 1.3 mg commercial catalyst, and C) with Pd NP-NS catalyst.

Mass spectrum collected from the reaction mixture of commercial catalyst showed a few orders of magnitude less intense peak at m/z 183 (the reaction product) as compared to the reaction mixture where Pd NP-NSs were used as catalyst (Figure S11). Hence, it is clear that Pd NP-NS showed higher catalytic efficiency than the commercially available Pd(0) catalyst.

Table S1. Structures of reactants and products.

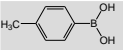

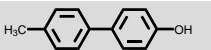


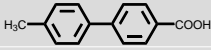









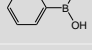
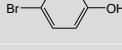
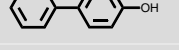
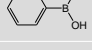
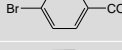

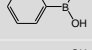
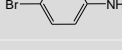
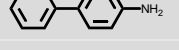
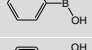
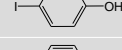
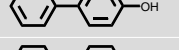



| Sl. No. | Reactant A | Reactant B | Product | <i>m/z</i> |
|---------|-----------------------------------------------------------------------------------|-----------------------------------------------------------------------------------|------------------------------------------------------------------------------------|------------|
| 1 |  |  |  | 183 |
| 2 |  |  |  | 211 |
| 3 |  |  |  | 184 |
| 4 |  |  |  | 183 |
| 5 |  |  |  | 211 |
| 6 |  |  |  | 169 |
| 7 |  |  |  | 197 |
| 8 |  |  |  | 169 |
| 9 |  |  |  | 169 |
| 10 |  |  |  | 197 |

Table S1 shows the chemical structures of reactants, products and *m/z* values of the product for all the entries. Figures S11 (serial number 2-5 above) and S12 (serial number 6-10 above) show mass spectra collected from the different reaction mixtures.

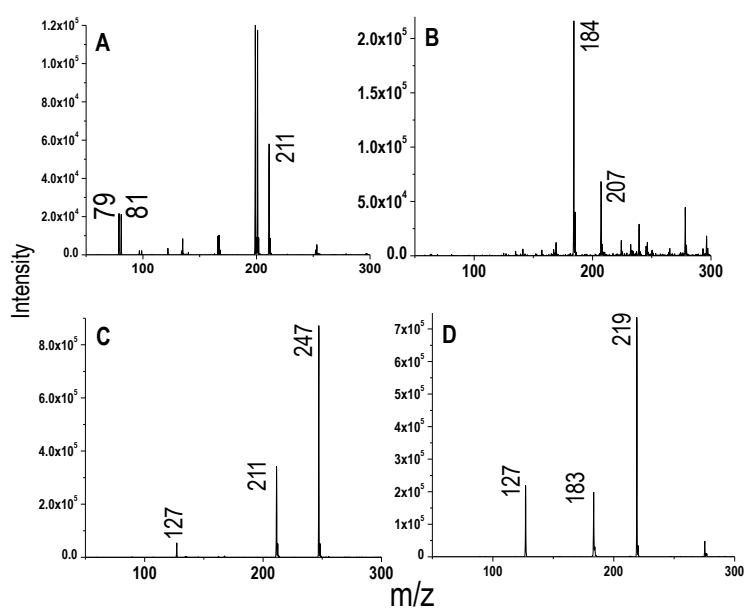


Figure S13. Mass spectrum collected from the reaction mixtures (serial no. 2-5) mentioned in Table S1.

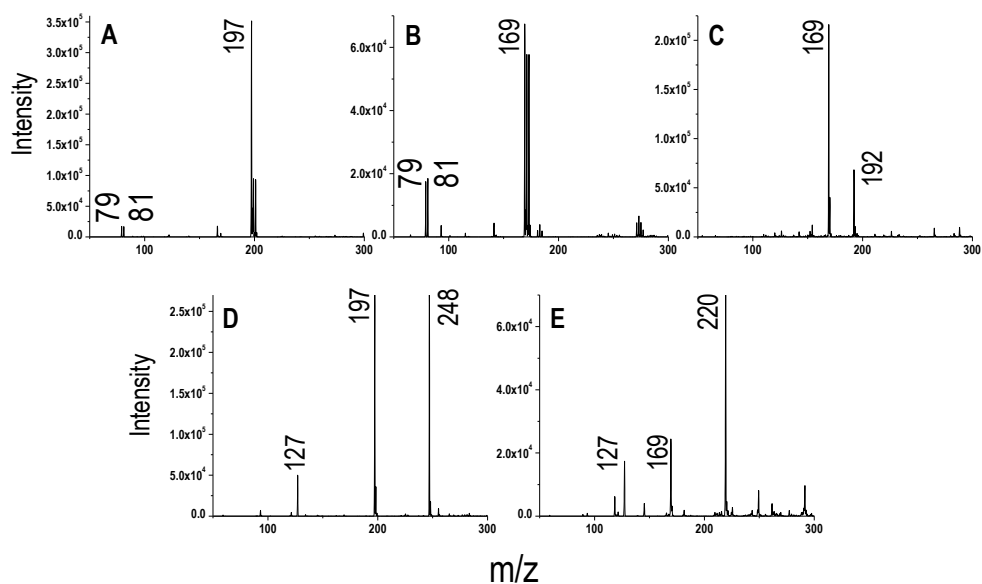


Figure S14. Mass spectrum collected from the reaction mixtures (serial no. 6-10) mentioned in Table S1.

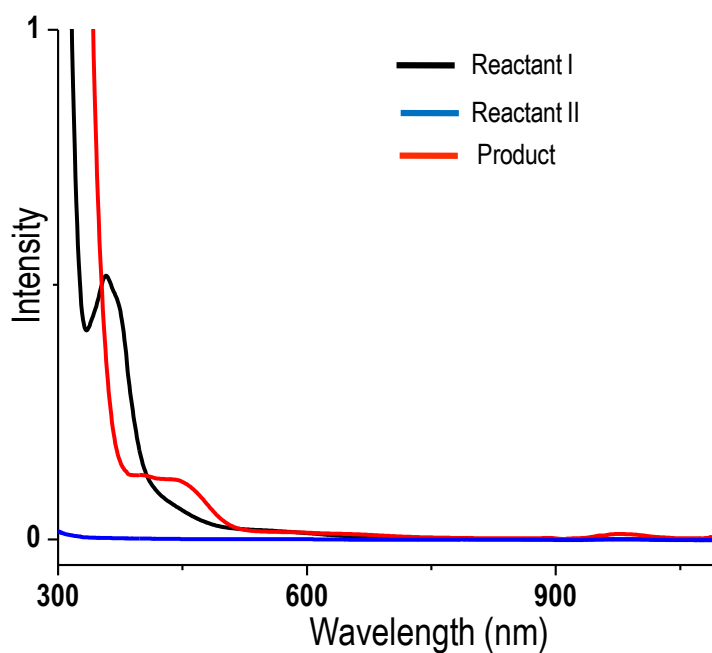


Figure S15. UV-Vis spectrum collected for the reactants and product. The black and blue traces are UV-Vis spectra of 4-iodophenol and 4-tolylphenylboronic acid, respectively.

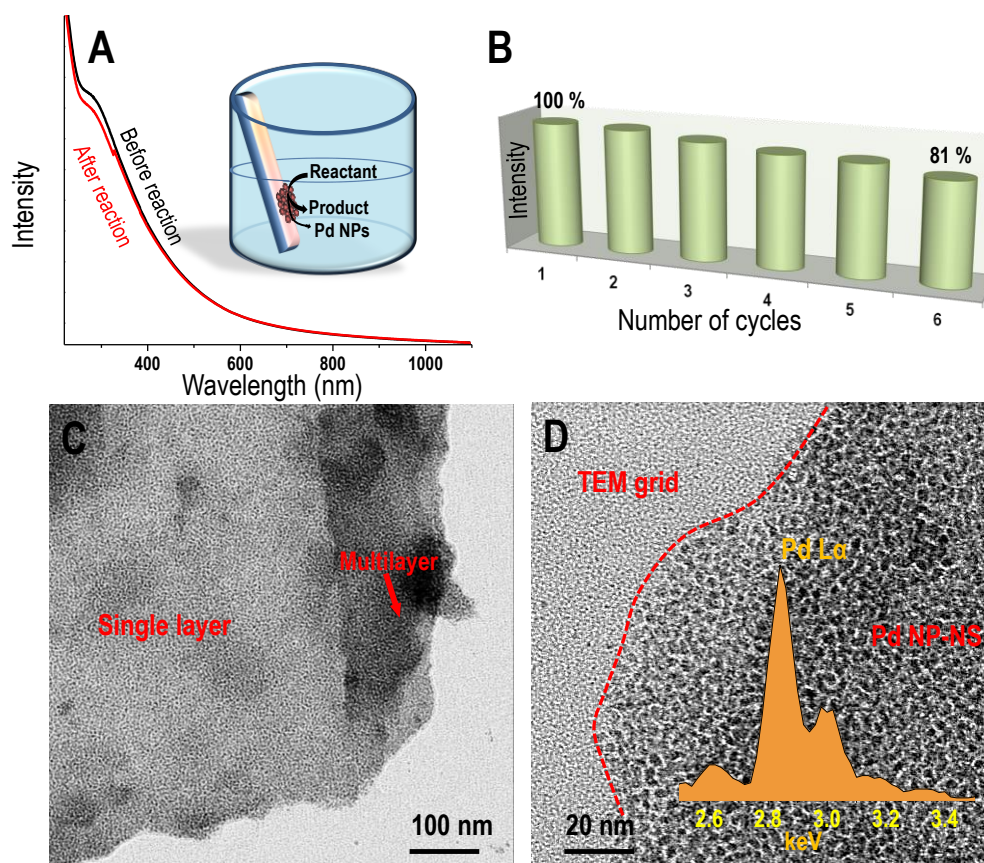


Figure S16. A) UV-Vis spectra of Pd NP-NS before and after the catalysis reaction, showing that catalysis does not change the nature of the sheet; inset shows a schematic representation of the catalysis experiment with minimal leaching of the Pd NPs into the reaction mixture. B) Intensity (absolute intensity of the product in mass spectrum) vs number of cycles for the same catalyst, showing that after 6 cycles also 81% of the catalytic activity was restored, C and D) TEM images of the Pd NP-NS after reaction showing that the nature of the sheet remains almost unchanged, inset in D shows the EDS spectrum taken from the same.

Reusability of the catalyst: Figure S14A shows the solid state UV-Vis spectrum of Pd NP-NS before and after catalysis. The spectrum was identical in both the cases. A small decrease in the intensity can be due to the loss of a small portion of Pd NP-NS while washing. Reusability of the catalyst was also checked. Figure S14B shows a plot of the absolute intensity of the product formed when the same catalyst was used again for a particular coupling reaction. Efficiency of the catalyst can be calculated taking the absolute intensity of the peak, in the mass spectrum, corresponding to the product. It proves

that after 6 cycles of catalysis reaction, about 81% of the catalytic activity was retained. Figure 5C and D show TEM images of the Pd NP-NSs after the reaction, proving that the NPs are intact and are similar in size. EDS spectrum of the Pd NP-NS after the reaction exhibits only Pd. These data prove that the Pd NP-NS act as a catalyst for the coupling reactions and the same catalyst can be reused for many reactions.

Theoretical details: In this section, we detail the theoretical method for obtaining the electrohydrodynamic flow described in the main text. In the experiment, free charged ions are sprayed using electrospray at the air-water interface of a container with an electrode on its surface. The electrospray of charges leads to a free charge density ρ on the interface between the two surfaces. The net current density at the air-water interface, in presence of flow v , is given as

$$J = \sigma E + \rho v \quad (1)$$

where σ is the conductivity of the liquid and E is the electric field intensity. In a homogeneous and incompressible fluid σ and ϵ are constant and $\nabla \cdot v = 0$. Using the continuity equation, given in the main text, we have

$$(\partial_t + v \cdot \nabla) \rho + \frac{\sigma}{\epsilon} \rho = 0 \quad (2)$$

This sets a relaxation time scale $\tau = \epsilon / \sigma$. The relaxation time in a fluid when surface charges is then obtained using the ratio of the dielectric constant and the conductivity¹. This has been used to estimate time scales in the main text. The estimated time scale is much faster than the remaining time scales and thus we conclude that there is electrohydrodynamic coupling only at the interface and not in the bulk.

The interfacial force density f^δ can be obtained from the electrical stress tensor $T_{ij}^e = \epsilon E_i E_j - 1/2 \epsilon E^2 \delta_{ij}$ as

$$f^{\delta} = \nabla \cdot T^e = \rho E - 0.5 E^2 \nabla \epsilon \quad (3)$$

Here we have used the Maxwell equation $\nabla \cdot D = \rho$, where $D = \epsilon E$ is the electric displacement vector, to obtain the above expression of interfacial force density. For a homogeneous system, ϵ is constant, and the second term in the above equation goes to zero. The expression of the interfacial force density f^{δ} on the interface is then given as

$$f^{\delta} = \rho E \quad (4)$$

We now use the above expression for the interfacial force density to obtain the fluid flow. The fluid flow v is obtained from the solution of the Stokes equation

$$\nabla \cdot v = 0, \quad \nabla \cdot T^m = 0 \quad (5)$$

where $T^m = -pI + \eta(\nabla v + (\nabla v)^T)$ is the fluid stress, p is the fluid pressure and η is the viscosity of the fluid. The above is then solved in a rectangular geometry of fluid flow, where the flow satisfies the no-slip condition on the two side walls and the bottom wall of a long rectangular container.

The boundary integral representation of the Stokes equation has been used to determine the flow². The explicit expression of the boundary integral representation of Stokes flow has been given in Eq.(4) of the main text. This is given in terms of a Green's function G which vanishes at the container walls. Then, the integral has contributions only from the interface. We assume a constant tangential electric field E and a Gaussian free charge density profile ρ at the interface. Finally, we neglect the second term of the integral, in Eq.(4) of the main text, as it is sub-dominant compared to the first term. With these assumptions, the integral can be completed and the streamlines of the flow can be numerically computed. The approximate solution of the flow at any point r in the bulk is then given as

$$v(r) = \int G(r, r') \cdot f^s(r') dS \approx \sum_j G(r, R_j) \cdot (Q \exp(-r^2/2a^2) E) \quad (6)$$

Here $f^s(r) = \rho E$ is the interfacial force density obtained in Equation 4. The integration is completed by considering the fact that the density of the charges can be written as $\rho(r) = \sum_j Q \delta(r - R_j) \exp(-r^2/2a^2)$, where a is the characteristic width and Q is the strength of charge. We ensure that the ratio a/H is consistent with the experiment. The Green's function G is obtained from the series sum of the Lorentz-Blake tensor³ about the side walls. The Lorentz-Blake tensor ensures no-slip condition at the bottom wall by construction, while the boundary condition at side walls is implemented by the series sum of the Lorentz-Blake tensor. The resulting flow expression is then computed numerically from Equation 6 to obtain the streamlines in Figure 3 of the main text.

Video of electrohydrodynamic fluid flow visualization:

Video S1. Electrohydrodynamic fluid flow, visualized using a dye (Rhodamine 6g) in a rectangular container. The file presents theoretical aspects in the beginning followed by a video of the experiment.

Video S2. Electrohydrodynamic fluid flow at the surface of the liquid, visualized using a dye (Rhodamine 6g) under UV light in a circular container.

References

1. Melcher, J. R.; Taylor, G. I., Electrohydrodynamics: A Review of the Role of Interfacial Shear Stresses. *Annual Review of Fluid Mechanics* **1969**, *1* (1), 111-146.
2. C. Pozrikidis, Boundary Integral and Singularity Methods for Linearized Viscous Flow, *Cambridge University Press, Cambridge*, **1992**.
3. Blake, J. R., A note on the image system for a Stokeslet in a no-slip boundary, *Proc. Camb. Phil. Soc.* **1971**, *70*, 303–310.